Magnetic resonance study of multiwall boron nitride nanotubes

A. M. Panich,[1,*] A. I. Shames,[1] N. Froumin,[2] C. C. Tang,[3] and Y. Bando[3]
[1]*Department of Physics, Ben-Gurion University of the Negev, Beer Sheva 84105, Israel*
[2]*Department of Materials Engineering, Ben-Gurion University of the Negev, Beer Sheva 84105, Israel*
[3]*Advanced Materials Laboratory, National Institute for Materials Science, 1-1 Namiki, Tsukuba 305-0044 Ibaraki, Japan*
(Received 27 December 2004; revised manuscript received 19 May 2005; published 2 August 2005)

We report on electron paramagnetic resonance (EPR) and ^{11}B nuclear magnetic resonance (NMR) study of multiwall boron nitride nanotubes. We measured the whole ^{11}B NMR spectrum in the external magnetic field of 8.0196 T and the central $\frac{1}{2}\rightarrow-\frac{1}{2}$ transition in 1.22 T. The quadrupole coupling constant and asymmetry parameter were determined from the splitting between satellites and by analysis of the line shape of the central transition. We show the closeness of these parameters in boron nitride nanotubes and bulk hexagonal BN. The spectra correspond to the axial symmetry of the boron site. EPR and x-ray photoelectron spectra are comparable to those of powder BN. The data obtained reflect a very similar local symmetry of the boron site and charge distribution over the B—N bond in nanotubes and bulk BN. These facts explain why BN nanotubes hold the electronic properties of the bulk compound.

DOI: 10.1103/PhysRevB.72.085307 PACS number(s): 61.46.+w, 76.60.−k, 76.30.−v

I. INTRODUCTION

Similar to carbon nanotubes, boron nitride (BN) nanotubes are quasi-one-dimensional nanostructures. However, their physical properties are different from those of carbon nanotubes. Carbon nanotubes exhibit metallic or semiconducting behavior depending on wrapping angle [or (n,m) index], while BN nanotubes are semiconductors irrespective of their helicity. Being chemically inert and oxidation and corrosion resistant, they are proving useful for applications in electronics. During recent years many theoretical predictions of BN nanotube properties such as piezoelectricity and the photogalvanic effect, as well as calculations of the Young modulus, band gap, etc., have been made.[1–5] Single- and multiwall BN nanotubes are predicted to be semiconductors with a wide energy gap (~5.5 eV) regardless of diameter, chirality, and coaxial arrangement.[1,2] However, experimental characterizations of the electronic properties of BN nanotubes are still insufficient.

In this paper, we report on the ^{11}B nuclear magnetic resonance (NMR), electron paramagnetic resonance (EPR), and x-ray photoelectron (XPS) studies of multiwall BN nanotubes. ^{11}B is a quadrupolar nucleus having spin $I=3/2$ and provides an excellent probe for studying the chemical bonding and local site symmetry by means of NMR. For such nuclei, the quadrupolar perturbed NMR spectrum consists of a central line and two satellites; the latter are usually difficult to detect in a powder sample. In our study, we measured the whole ^{11}B NMR spectrum in the external magnetic field of 8.0196 T and separately the central $\frac{1}{2}\rightarrow-\frac{1}{2}$ transition in 1.22 T. The quadrupole coupling constant (QCC) and asymmetry parameter were determined from the splitting between satellites and by analysis of the line shape of the central transition. Our data show a strong resemblance of these parameters in BN nanotubes and bulk hexagonal BN (h-BN). The spectra correspond to the axial symmetry of the boron site. EPR and XPS spectra are found to be similar to those of powder BN. The data obtained are discussed along with the published theoretical and experimental results and explain why BN nanotubes show the same electronic properties as the bulk compound.

II. EXPERIMENTAL DETAILS

All experiments were performed on macroscopic powder samples of multiwall BN nanotubes. The details of the preparation method can be found elsewhere.[6,7] Typical scanning (SEM) and transmission (TEM) electron microscope images of the multiwall BN nanotubes under study are given in Fig. 1. The averaged inner diameter of the nanotubes as measured over several TEM pictures is around 7 nm with a standard deviation of 3 nm. Most tubes have a length about 1–2 μm and the number of walls ~20 ranging from 8 to 40 layers.

X-ray photoelectron spectroscopy analysis was performed using a PHI 549 SAM/AES/XPS ultrahigh-vacuum (10^{-9} torr) apparatus with double cylindrical mirror analyzer and Mg $K\alpha$ (12 536 eV) x-ray source. A powder BN nanotube sample was mounted on an indium foil. High-resolution B and N spectra were taken at pass energy 25 eV. The spectra (Fig. 2) show rather narrow (~1.6 eV full width at half maximum) symmetric B 1s and N 1s peaks at 190 and 400 eV, respectively. The obtained peak positions are practically the same as those reported in powder h-BN.[8]

Room-temperature EPR spectra were recorded with a Bruker EMX-220 digital X-band (ν=9.4 GHz) EPR spectrometer. Calibration of the g factor was done by simultaneous recording of the BN nanotube sample and a capillary tube containing 30 μM water solution of stable nitroxide 4–hydroxy tempo radical (TEMPOL) with $g=2.0059\pm0.0001$. Concentration of paramagnetic centers was evaluated with respect to the calibrated weak pitch sample. Postprocessing and simulation of EPR spectra were done using Bruker's WIN-EPR and SIMFONIA software and then EPR parameters were optimized by NIEHS's (National Institute of Environmental Health Sciences) WINSIM software.

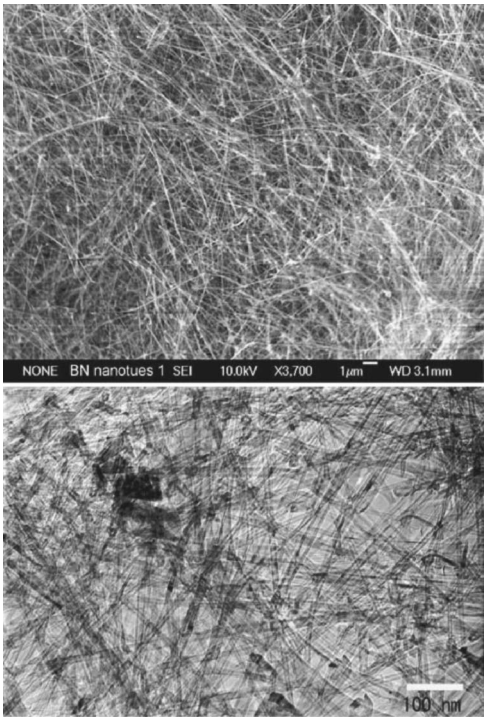

FIG. 1. SEM and TEM images of the multiwall BN nanotubes.

^{11}B NMR spectra and spin-lattice relaxation measurements were carried out using Tecmag LIBRA and Tecmag APOLLO pulse solid state NMR spectrometers. The spectra were measured in the external magnetic fields of 1.22 and 8.0196 T. The low-field spectrum was obtained from Fourier transformation of the spin echo using a 16-phase cycling sequence, while the wide-spanned high-field spectra were recorded using a frequency-shifted and summed Fourier transform processing technique[9] in the temperature range 77–292 K. The spin-lattice relaxation time T_1 was measured by means of a saturation comb sequence. The duration of the $\pi/2$ pulse was 3.7 μs at resonance frequency 109.5 MHz and 5.2 μs at 16.7 MHz. We note that the NMR signal in a BN nanotube sample was maximized by the pulse length close to one-half of that maximizing the ^{11}B signal in a liquid boron trifluoride methanol complex $(CH_3OH)_2$-BF_3, as must occur for the spin-3/2 quadrupole nuclei.[10]

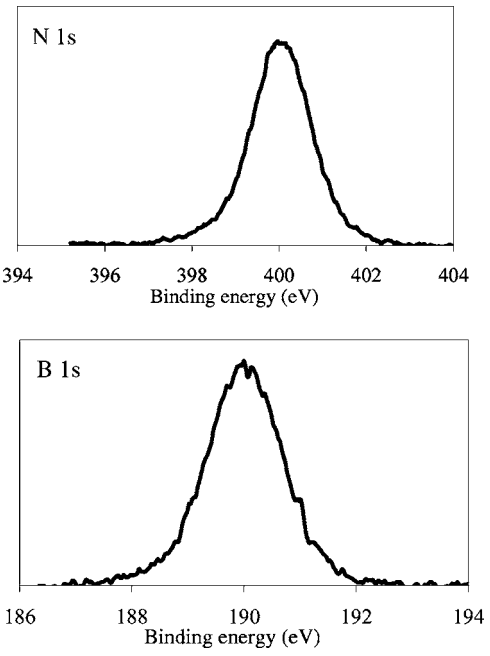

FIG. 2. Boron 1*s* and nitrogen 1*s* XPS spectra.

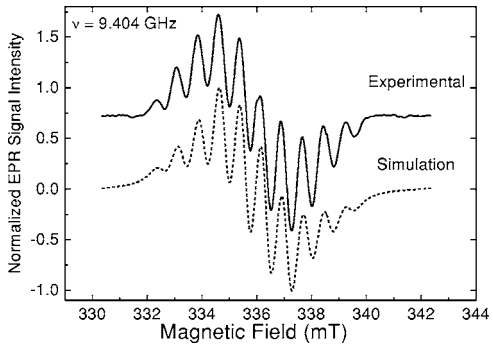

FIG. 3. Room-temperature EPR spectra of boron nitride nanotubes, ν=9.404 GHz: experimental results (solid line) and spectrum simulation (dashed line).

III. RESULTS

A. EPR spectra

EPR measurements were carried out in order to get information on the presence and local structure of paramagnetic centers. The wide-span EPR spectrum of the BN nanotube sample shows superposition of a very weak broad line and a sharp intense EPR signal located in the vicinity of g=2.00. The latter signal shows splitting into ten well-resolved lines (Fig. 3, experimental). The broad signal (not shown) may be attributed to a minute amount of paramagnetic impurities, whereas the sharp one is due to the unpaired electron trapped in a nitrogen vacancy, which is surrounded by m=3 equivalent boron atoms. Since the natural abundance of ^{11}B nuclei is 80.1%, just these nuclei make their contribution to the resolved hyperfine structure:[11] the number of hyperfine components is $N=2I(^{11}\mathrm{B})m+1=10$, where $I(^{11}\mathrm{B})=3/2$. The experimental spectrum was simulated using Lorentzian shapes of the hyperfine lines with ΔH_{pp}=0.48 mT, taking into account the natural abundance of both (^{11}B and ^{10}B) boron isotopes (Fig. 3, simulation). It was found that nuclei of the second isotope with $I(^{10}\mathrm{B})=3$ only weakly affect the signal line shape, adding a broad singlet line to the center of the well-resolved ten-line hyperfine envelope. The simulation results in hyperfine splitting constants $A_{iso}(^{11}\mathrm{B})=0.76\pm0.01$ mT, $A_{iso}(^{10}\mathrm{B})\sim0.15$ mT, and $g_{iso}=2.0032\pm0.0005$. The spin concentration was evaluated as $\sim9\times10^{15}$ spins/g. A similar spectrum with $A=0.78\pm0.01$ mT apart from a g value of 2.0027 ± 0.0003 has been observed in bulk *h*-BN irradiated by x, uv, and γ radiation and heated to 1850 °C.[11,12] A recent investigation of *h*-BN made by Fanciulli[13] shows very similar results. Our conclusion on the

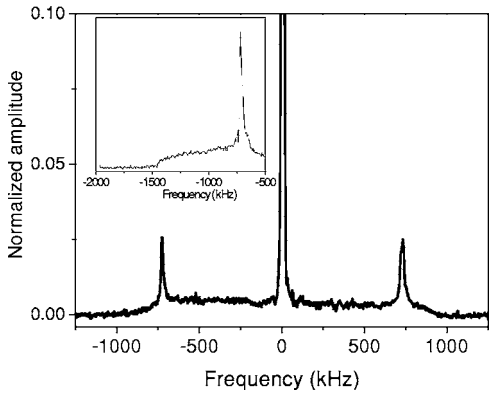

FIG. 4. Room-temperature ^{11}B NMR spectrum in magnetic field $B_0=8.0196$ T. In inset, separately measured low-frequency part of the spectrum is given.

contribution of the ^{10}B isotope to the EPR spectrum is also in accordance with those works. We note that the EPR spectra of cubic modifications of boron nitride[13–15] do not exhibit hyperfine structure; for a detailed discussion, the reader is referred to Ref. 13.

B. NMR spectra and spin-lattice relaxation

^{11}B is a quadrupolar nucleus having spin $I=3/2$. The spin Hamiltonian for the ^{11}B in BN is

$$\begin{aligned}\mathcal{H} &= \mathcal{H}_z + \mathcal{H}_Q + \mathcal{H}_{\mathrm{dip}} \\ &= -\gamma_n \hbar B_0 I_z + [e^2qQ/4I(2I-1)][3I_z^2 - I^2 + \eta(I_x^2 - I_y^2)] \\ &\quad + \mathcal{H}_{\mathrm{dip}}. \end{aligned} \tag{1}$$

Here the first term is the nuclear Zeeman interaction with the external magnetic field $B_0 \| z$, and the second term describes the quadrupole interaction; eq is the electric field gradient (EFG), eQ is the nuclear electric quadrupole moment, and η is the asymmetry parameter. The last term represents the dipolar interaction of ^{11}B with the other nuclei; it does not contribute much to the spectra. If $\mathcal{H}_z \gg \mathcal{H}_Q$, the quadrupole interaction can be treated as a perturbation to the Zeeman interaction. For a spin-3/2 nucleus, the quadrupolar perturbed NMR spectrum consists of three transitions. The first-order effects do not affect the central $\frac{1}{2} \rightarrow -\frac{1}{2}$ transition that is observed at the Larmor frequency ν_L, while two satellite lines ($3/2 \rightarrow 1/2$ and $-1/2 \rightarrow -3/2$ transitions) are shifted to frequencies determined by the product of $\nu_Q = e^2qQ/2h$ and an angular function related to the orientation of the applied magnetic field in the EFG principal axis frame. In a powder, the satellite lines are distributed over the frequency range of the order of $2\nu_Q$ with the singularities at $\pm\nu_Q/2$ and shoulders at $\pm\nu_Q$ that are rather difficult to detect. Nevertheless, the experimental ^{11}B NMR spectrum, given in Fig. 4, readily shows the aforementioned structure. From the distance between satellites, the room-temperature values of ν_Q and quadrupole coupling constant e^2qQ/h were found to be 1.453 and 2.906 MHz, respectively. Neither a splitting nor any unexpected broadening of the satellite transitions is observed, leading to the conclusion of a zero value of the asymmetry parameter η.

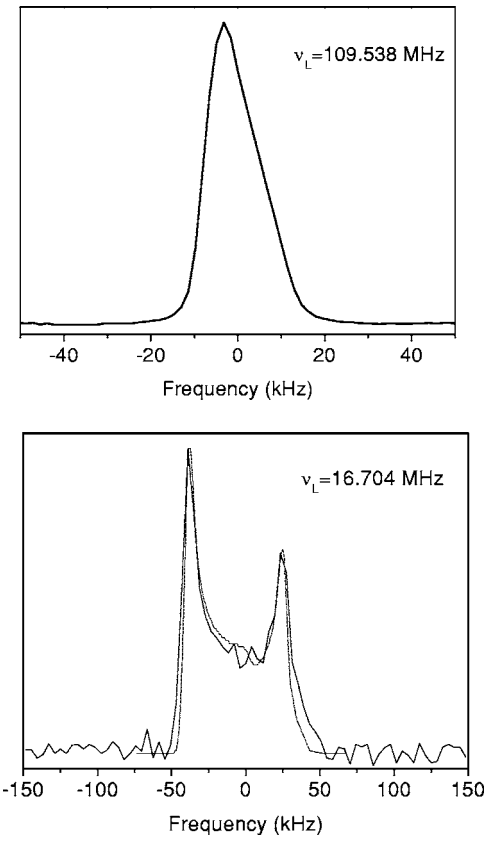

FIG. 5. Central line ($1/2 \rightarrow 1/2$ transition) of the room-temperature ^{11}B NMR spectra measured in magnetic field $B_0=8.0196$ T and resonance frequency $\nu_0=109.538$ MHz (top) and $B_0=1.22$ T and $\nu_0=16.704$ MHz (bottom). Simulated spectrum corresponding to zero asymmetry parameter η is shown by dotted line.

The shape of the central line ($\frac{1}{2} \rightarrow -\frac{1}{2}$ transition) is determined by the second-order effects and shows several singularities. For trigonal and higher symmetry, when $\eta=0$, its shape in a powder sample is given by[16]

$$\begin{aligned} &[(5+3z)^{-1/2} + (5-3z)^{-1/2}]/4z \quad \text{for } \nu_L - 16B/9 \leqslant \nu \leqslant \nu_L, \\ &(5-3z)^{-1/2}/4z \quad \text{for } \nu_L \leqslant \nu \leqslant \nu_L + B, \\ &0 \quad \text{otherwise}, \end{aligned} \tag{2}$$

where $z=[16/9+(\nu-\nu_L)/B]$,[1,2] and $B=[I(I+1)-3/4]\nu_Q^2/16\nu_L$. The line shape exhibits two singular points at $\nu=\nu_L-16B/9$ and $\nu=\nu_L+B$, and the quadrupole coupling frequency ν_Q can be determined from the difference Δ between the singularities of the powder spectrum. For $I=3/2$, $\Delta=25B/9=25\nu_Q^2/48\nu_L$.

The central lines ($\frac{1}{2} \rightarrow -\frac{1}{2}$ transitions) of the experimental room-temperature ^{11}B NMR spectra at resonance frequencies 109.538 and 16.704 MHz are shown in Fig. 5. At high resonance frequency the splitting Δ, being reciprocally proportional to ν_L, is rather small, and the aforementioned singularities are not seen, being broadened by the dipole-dipole interaction. However, they are well seen at low resonance frequency, showing a classic line shape caused by the

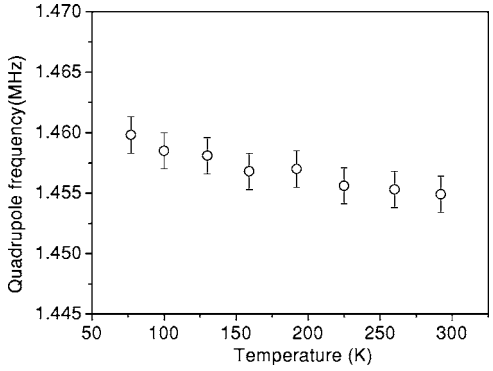

FIG. 6. Temperature dependence of the quadrupole frequency.

second-order quadrupolar effect with a zero asymmetry parameter η. The separation between two peaks, observed at $\nu_L = 16.7$ MHz, was found to be $\Delta = 63.5$ kHz. Using Eq. (2), one can evaluate $\nu_Q = 1.427$ MHz and $e^2qQ/h = 2.854$ MHz, which are in a good agreement with those values obtained above from the satellite positions. The average value from the two aforementioned measurements yields $e^2qQ/h = 2.880 \pm 0.026$ MHz.

Let us now consider the variation of the quadrupole frequency in BN nanotubes as a function of temperature. Bayer[17] and Kushida *et al.*[18] have shown that temperature dependence of ν_Q is given by the expression

$$\nu_Q = \nu_0(1 - bT - c/T) \tag{3}$$

where $b = (3k/2)\Sigma(A_i/\omega_i^2)$, $c = (h^2/8k)\Sigma A_i$, ω_i is the frequency of the ith mode of vibration, k is Boltzmann's constant, and A_i^{-1} has the dimension and order of magnitude of the moment of inertia of the ith mode of vibration. According to this theory, the average EFG at the nucleus usually decreases with increasing temperature solely because of the increase in the amplitude of the thermal vibrations. The major contribution comes from the low-frequency ($\omega < 100$ cm^{-1}) torsional vibrations that are especially large in molecular crystals. In the layered h-BN, however, such vibrations are absent. Out-of-plane acoustical modes, also included with the low-frequency terms, cause very small changes of EFG (less than 1%) in the temperature range 4.2–300 K. The contribution of the high-frequency ($\omega > 1000$ cm^{-1}) in-plane vibrations is much less than that of the low-frequency terms and is neglected in practice.[18] Therefore the internal dynamics of boron nitride should be essentially due to zero-point vibrations. The quadrupole frequency in h-BN, measured at liquid helium temperature,[19,20] was found to be 1.467 kHz. This value practically coincides with that measured at ambient temperature and confirms the temperature independence of ν_Q in h-BN. One can expect the same effect for the multiwall BN nanotubes under study. This is readily confirmed by our experiment (Fig. 6), which shows practically negligible temperature dependence of the quadrupole frequency.

Boron spin-lattice relaxation measurements (Fig. 7) yield a very long relaxation time. In the presence of paramagnetic

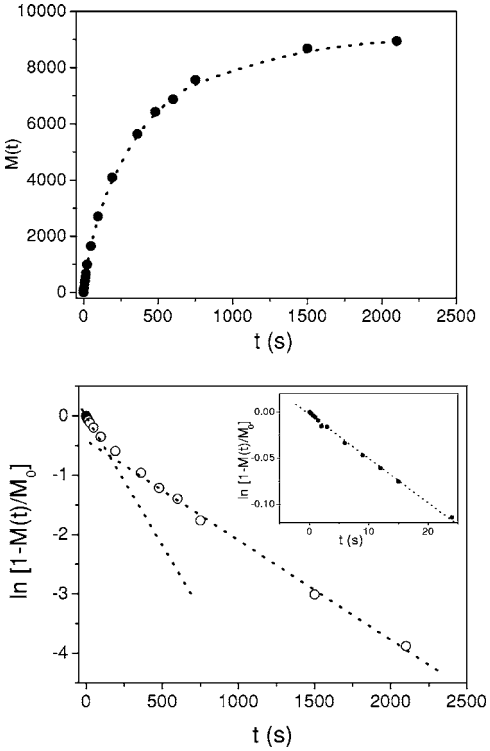

FIG. 7. ^{11}B magnetization recovery in the linear (top) and half-logarithmic (bottom) scales. Resonance frequency $\nu_0 = 109.58$ MHz. Dashed lines show two-exponential fit Eq. (4). In inset, the initial part of $M(t)$ corresponding to the faster component is shown.

centers described above, ^{11}B nuclear magnetization recovery should be fitted by a stretched exponential.[21] However, bringing the amount of these centers (determined by means of EPR) into correlation with the estimated number of nanotubes, one can come to the conclusion that the number of paramagnetic centers is less than the number of the nanotubes, so that there are nanotubes either with or without paramagnetic centers. Since spin diffusion between different nanotubes is unlikely, in such a case the ^{11}B magnetization recovery should be fitted by a superposition of two exponentials:

$$M(t) = M_1(0)\{1 - \exp[-(t/T_{11})^{\alpha}]\} + M_2(0)[1 - \exp - (t/T_{12})], \tag{4}$$

where the first term (stretched exponential) is assigned to the nanotubes in which the relaxation via paramagnetic centers is a dominant mechanism. The corresponding fit is shown in Fig. 7, yielding $T_{11} = 76 \pm 13$ s, $\alpha = 0.86 \pm 0.03$, and $T_{12} = 495 \pm 21$ s.

An alternative possibility for explaining our data assumes that the two-exponential fit of the ^{11}B magnetization is caused by a combination of contributions of $\Delta m = 1$ and 2 transitions. However, in powder samples the corresponding transition probabilities are usually the same,[22,23] and a single-exponential recovery is essentially observed.

TABLE I. Quadrupole coupling constants of bulk *h*-BN and BN nanotubes at ambient temperature.

Compound	e^2qQ/h (MHz)	Reference
Bulk *h*-BN	2.96±0.10	25
Bulk *h*-BN	2.9	26
Bulk *h*-BN	3.00±0.10	23
Bulk *h*-BN	2.936±0.020	27
BN nanotubes	2.880±0.026	This paper

IV. DISCUSSION

Recently published NMR spectra on BN nanotubes[24] were interpreted as two components arising from the hexagonal and rhombohedral phases. The distance between the components, supposedly assigned to these two phases, was shown to diminish with increased magnetic field. This fact strongly contradicts the NMR fundamentals (the larger the applied magnetic field the better the resolution between the signals). We have shown above that another mechanism, namely, quadrupole coupling, determines the line shape. Furthermore, we have shown that the faster component in relaxation measurements is due to the paramagnetic defects.

Let us first compare the value of the quadrupole coupling constant e^2qQ/h of BN nanotubes determined above with that of the hexagonal modification of bulk boron nitride (*h*-BN). The corresponding values[23,25–27] are given in Table I. One can find that the obtained value of $\nu_Q = 2.880 \pm 0.026$ MHz in nanotubes is only a little bit (2.4%) smaller than that of *h*-BN (the latter was found as an average value of the data given in Table I). Furthermore, the nanotube structure shows an axial symmetry of the boron site as in bulk *h*-BN. We note that the quadrupole coupling constant is particularly sensitive to variations of the chemical bonding and electron charge distribution in the neighborhood of the nucleus. The charges close to the nucleus have the most important effect. A closed shell with a spherically symmetric electronic charge contributes nothing to quadrupole coupling, and the contribution of the ionic bond vanishes. The essential QCC value of BN reflects a considerable covalency of the BN bond. Based on the Pauling electronegativities[28] ($x_B = 2.0$ and $x_N = 3.0$ for boron and nitrogen, respectively), one can estimate that a single B-N bond is expected to have 78% covalent character. Analysis of NMR data led to a conclusion of a charge transfer of 55%.[23,25] Due to the higher electronegativity of nitrogen as compared to boron, a charge transfer from boron to nitrogen takes place, and the bond density is polarized toward the nitrogen. The closeness of the QCC and η values of the multiwall BN nanotubes under study to those of bulk *h*-BN reflects very similar chemical bonding, local symmetry, and charge distribution over the B-N bond. This fact should result in similar electronic properties dominated by the band structure of the hexagonal-like BN sheets. That is why BN nanotubes are semiconductors with a nearly constant energy gap of 5.5 eV regardless of diameter, chirality, or the number of walls of the tube,[2] and their gap is close to that of bulk *h*-BN. The experimental value of the latter is ~5.8 eV,[29] while the calculated value is around 5.4–5.5 eV.[29,30] We note that calculations show very small variations in the bond lengths with the tube radius.[31] The calculated B-N bond length in nanotubes is found to be 1.438 Å,[31] which is almost coincident with the experimental value in bulk *h*-BN [1.446 Å (Ref. 32)]. One can expect that only BN nanotubes with very small diameter would show different electronic properties with respect to those of bulk *h*-BN and a decrease of the band gap caused by the curvature of the sheets and the appearance of some $sp^2 \rightarrow sp^3$ rehybridization.

A similar conclusion can be derived from the analysis of the EPR spectra. The close similarity of the line shapes, *g* factors, and hyperfine splitting parameters *A* reflects the same origin and local symmetry of the paramagnetic centers and nearly the same bond length and charge distribution in nanotubes and bulk *h*-BN. The same binding energy obtained by the XPS measurements in bulk and nanotube BN samples reflects the similar bonding and molecular orbital structure.

In summary, our data explain why BN nanotubes hold the electronic properties of the bulk compound. It allows us to suggest that a centrosymmetrical structure is also kept; thus one should be careful in predicting piezoelectricity in BN nanotubes which seems to be unlikely here.

ACKNOWLEDGMENT

We thank E. A. Katz for helpful discussions.

*Corresponding author. FAX: +972-8-6472903. Email address: pan@bgumail.bgu.ac.il

[1] A. Rubio, J. L. Corkill, and M. Cohen, Phys. Rev. B **49**, 5081 (1994).

[2] X. Blase, A. Rubio, S. G. Louie, and M. L. Cohen, Europhys. Lett. **28**, 355 (1994).

[3] E. J. Mele and P. Kral, Phys. Rev. Lett. **88**, 056803 (2002).

[4] S. M. Nakhmanson, A. Calzolari, V. Meunier, J. Bernholc, and M. B. Nardelli, Phys. Rev. B **67**, 235406 (2003).

[5] E. Hernandez, C. Goze, P. Bernier, and A. Rubio, Phys. Rev. Lett. **80**, 4502 (1998).

[6] C. Tang, Y. Bando, T. Sato, and K. Kurashima, Chem. Commun. (Cambridge) **2002**, 1290.

[7] C. C. Tang, Y. Bando, and D. Golberg, J. Solid State Chem. **177**, 2674 (2004).

[8] Y. M. Shulga, T. M. Moravskaya, S. V. Gurov, V. I. Chukalin, and Y. G. Borod'ko, Poverkhnost **10**, 155 (1990).

[9] W. G. Clark, M. E. Hanson, and F. Lefloch, Rev. Sci. Instrum. **66**, 2453 (1995).

[10] E. Fukushima and S. B. W. Roeder, *Experimental Pulse NMR: A Nuts and Bolts Approach* (Addison-Wesley, Reading, MA, 1981), pp. 109–111.

[11] G. Romelt, Z. Naturforsch. A **21**, 1970 (1966).
[12] D. Geist and G. Romelt, Solid State Commun. **2**, 149 (1964).
[13] M. Fanciulli, Philos. Mag. B **76**, 363 (1997).
[14] K. Atobe, M. Honda, M. Ide, H. Yamaji, T. Matsukawa, N. Fukuoka, M. Okada, and M. Nakagawa, Jpn. J. Appl. Phys., Part 1 **32**, 2102 (1993).
[15] M. Fanciulli and T. D. Moustakas, Physica B **185**, 228 (1993).
[16] M. H. Cohen and F. Reif, Solid State Phys. **5**, 321 (1957).
[17] H. Bayer, Z. Phys. **130**, 227 (1951).
[18] T. Kushida, G. B. Benedek, and N. Bloembergen, Phys. Rev. **104**, 1364 (1956).
[19] C. Connor, J. Chang, and A. Pines, J. Chem. Phys. **93**, 7639 (1990).
[20] M. P. Augustine, D. M. TonThat, and J. Clarke, Solid State Nucl. Magn. Reson. **11**, 139 (1998).
[21] W. E. Blumberg, Phys. Rev. **119**, 79 (1960).
[22] A. Rigamonti, Adv. Phys. **33**, 115 (1984).
[23] M. Fanciulli and M. Corti, Phys. Rev. B **52**, 11872 (1995).
[24] J. K. Jung, K.-S. Ryu, Y. Kim, and C. Tang, Solid State Commun. **130**, 45 (2004).
[25] A. H. Silver and P. J. Bray, J. Chem. Phys. **32**, 288 (1960).
[26] P. S. Marchetti, D. Kwon, W. R. Schmidt, L. V. Interrante, and G. E. Maciel, Chem. Mater. **3**, 482 (1991).
[27] G. Jeschke, W. Hoffbauer, and M. Jansen, Solid State Nucl. Magn. Reson. **12**, 1 (1998).
[28] L. Pauling, *The Nature of the Chemical Bond* (Cornell University Press, Ithaca, NY, 1960).
[29] A. Zunger, A. Katzir, and A. Halperin, Phys. Rev. B **13**, 5560 (1976).
[30] X. Blase, A. Rubio, S. G. Louie, and M. L. Cohen, Phys. Rev. B **51**, 6868 (1995).
[31] B. Akdim, R. Pachter, X. Duan, and W. W. Adams, Phys. Rev. B **67**, 245404 (2003).
[32] R. S. Pease, Acta Crystallogr. **5**, 356 (1952).